Available online at www.sciencedirect.com
SCIENCE DIRECT®
ELSEVIER Applied Mathematics and Computation 174 (2006) 795–809
APPLIED MATHEMATICS AND COMPUTATION
www.elsevier.com/locate/amc

Analytical and numerical study of nonlinear effects at tsunami modeling

Narcisse Zahibo [a], Efim Pelinovsky [a,b,*], Tatiana Talipova [b], Andrey Kozelkov [c], Andrey Kurkin [c]

[a] *Département de Physique, Université des Antilles et de la Guyane, UFR Sciences, Campus de Fouillole, 97159 Pointe à Pitre Cedex, Guadeloupe, France*
[b] *Laboratory of Hydrophysics and Nonlinear Acoustics, Institute of Applied Physics, 46 Uljanov Street, Nizhny Novgorod 603950, Russia*
[c] *Department of Applied Mathematics, Nizhny Novgorod Technical University, 24 Minin Street, Nizhny Novgorod 603950, Russia*

Abstract

The giant tsunami occurred in the Indian Ocean on 26th December 2004 pays attention to this natural phenomenon and the possibility to use the analytical methods. The given paper demonstrates the role of nonlinear effects in the computed dynamics of the tsunami waves in shallow seas and the applicability of the rigorous and approximated solutions of the nonlinear theory of water waves to explain the results of the numerical simulation.

Keywords: Nonlinear hyperbolic systems; Nonlinear waves; Tsunamis; Perturbation method; Numerical simulation

* Corresponding author. Address: Laboratory of Hydrophysics and Nonlinear Acoustics, Institute of Applied Physics, 46 Uljanov Street, Nizhny Novgorod 603950, Russia.
E-mail addresses: narcisse.zahibo@univ-ag.fr (N. Zahibo), pelinovsky@hydro.appl.sci-nnov.ru (E. Pelinovsky).

0096-3003/$ - see front matter © 2005 Elsevier Inc. All rights reserved.
doi:10.1016/j.amc.2005.05.014

1. Introduction

Tsunami waves are defined as surface gravity waves that occur in the ocean as the result of large-scale short-term perturbations (underwater earthquakes, eruptions of underwater volcanoes, landslides, rock falls, pyroclastic avalanche from land volcanoes entered in water, asteroid impact, underwater explosions, etc); see for instance, Murty [9], Pelinovsky [12] and Bryant [1]. Tsunamis' characteristic parameters are: duration, 5–100 min, length, 100 m–1000 km, propagation speed, 1–200 m/s, and their heights can be up to tens of meters. Tsunami waves of the seismic origin are usually very long (50–1000 km), for instance the source of the giant 2004 tsunami in the Indian Ocean (magnitude 9.0–9.3) has approximated dimensions: length, 670 km; width, 150 km; and height, 12 m [10,21]. Taking into account that the characteristic wavelength exceeds the water depth, the popular models to describe the tsunami propagation are based on the various approximations of the shallow-water system. The Earth sphericity and rotation are essential for tsunami waves in the open ocean, and here the basic shallow-water system becomes

$$\begin{aligned} &\frac{\partial M}{\partial t}+\frac{gh}{R\cos\theta}\frac{\partial \eta}{\partial \varphi}=fN, \quad \frac{\partial N}{\partial t}+\frac{gh}{R}\frac{\partial \eta}{\partial \theta}=-fM,\\ &\frac{\partial \eta}{\partial t}+\frac{1}{R\cos\theta}\left[\frac{\partial M}{\partial \varphi}+\frac{\partial}{\partial \theta}(N\cos\theta)\right]=0, \end{aligned} \tag{1}$$

where θ and φ are latitude and longitude, R is the radius of the Earth, $f=2\omega_e\sin(\theta)$ is the Coriolis parameter, ω_e is the Earth rotation frequency, M and N are discharge fluxes along the latitude and longitude, $h(x,y)$ is unperturbed basin depth. This model can be applied to compute the tsunami waves on long distances (1000–10 000 km). In particular, the numerical simulation of two global tsunamis in the Indian Ocean (1883 Krakatau volcano eruption, and 2004 Indonesian earthquake), when the waves crossed the Indian Ocean and penetrated in the Pacific and Atlantic Oceans have been performed in the framework of this linear spherical model [3,21].

In the coastal zone and seas, having relative small scales (up to 1000 km), the model of plane Earth with no rotation is applied

$$\begin{aligned} &\frac{\partial M}{\partial t}+\frac{\partial}{\partial x}\left(\frac{M^2}{D}\right)+\frac{\partial}{\partial y}\left(\frac{MN}{D}\right)+gD\frac{\partial \eta}{\partial x}+\frac{k}{2D^2}M\sqrt{M^2+N^2}=0,\\ &\frac{\partial N}{\partial t}+\frac{\partial}{\partial x}\left(\frac{MN}{D}\right)+\frac{\partial}{\partial y}\left(\frac{N^2}{D}\right)+gD\frac{\partial \eta}{\partial y}+\frac{k}{2D^2}N\sqrt{M^2+N^2}=0,\\ &\frac{\partial \eta}{\partial t}+\frac{\partial M}{\partial x}+\frac{\partial N}{\partial y}=0, \end{aligned} \tag{2}$$

where $D=h(x,y)+\eta$ is the total water depth, M and N are discharge fluxes along the horizontal coordinates, x and y, and $k=0.0025$ is the bottom friction

coefficient (the same value is used in the theory of tidal waves). Nonlinear effects within the hyperbolic system (2) are evident, and they lead to the shock wave formation (bore). Meanwhile, in the tsunami practice, such processes are studying usually for runup stage [16,11,13,2], or for tsunami waves entered in the river mouth [17]; and the famous Hokusai's painting of the breaking wave on the coast is now the tsunami image. There is a few of papers with estimation of the role of nonlinear effects at the tsunami propagation [7,8,15]; in many numerical simulations the grid resolution in the offshore zone is large (100–2000 m) and can not provide the good description of the shock structure of the tsunami wave.

The main goal of this paper is to study the applicability of the analytical methods to describe nonlinear effects at tsunami modeling in shallow seas. The numerical simulation of the tsunami waves in the Java Sea (where tsunami is a very often phenomenon) is performed with use of numerical code TUNAMI developed in Tohoku University. The obtained results are described in Section 2. The role of nonlinear effects in the source area is investigated in the framework of the shallow-water theory analytically in Section 3; and far from the source in Section 4. Results of the analytical 1D solutions of the hyperbolic system are in good comparison with 2D numerical simulations (Section 5). Obtained results are discussed in Conclusion.

2. Modeling of tsunami propagation within 2D hydrodynamic equations

The numerical simulation of tsunami waves in the framework of the 2D hyperbolic system (2) is now the routine work in the tsunami practice, and the various numerical codes are applied to determine tsunami characteristics. One of them is TUNAMI developed in Tohoku University (Japan) and provided through the Tsunami Inundation Modeling Exchange (TIME) program, see Goto et al. [6]. This model is very often used to simulate real events; in particular, authors applied it to study tsunami events in Mediterranean, Caribbean and Black Seas [14,18,19].

To demonstrate the role of the nonlinear effects in the tsunami wave field dynamics, we chose the shallowest Java Sea (Fig. 1) where the earthquakes generated the large tsunami waves several times. The bathymetry of the Java Sea is taken from GEBCO (British Oceanographic Data Center) with mesh grid of 1 km. Boundary conditions on the land correspond to the full reflection (vertical wall approximation) and on the open boundaries—to free passage of the waves.

The tsunami source is modeled by the ellipsoid with semi-axes 60 on 20 km and the height 1 or 5 m. Its center is located in the point with coordinates: 112.34E, 5.79S, the water depth in epicenter is 40 m. Such parameters correspond to the typical conditions of the tsunami source, and we will not discuss here the geophysical aspects of chosen source. The snapshots of the water

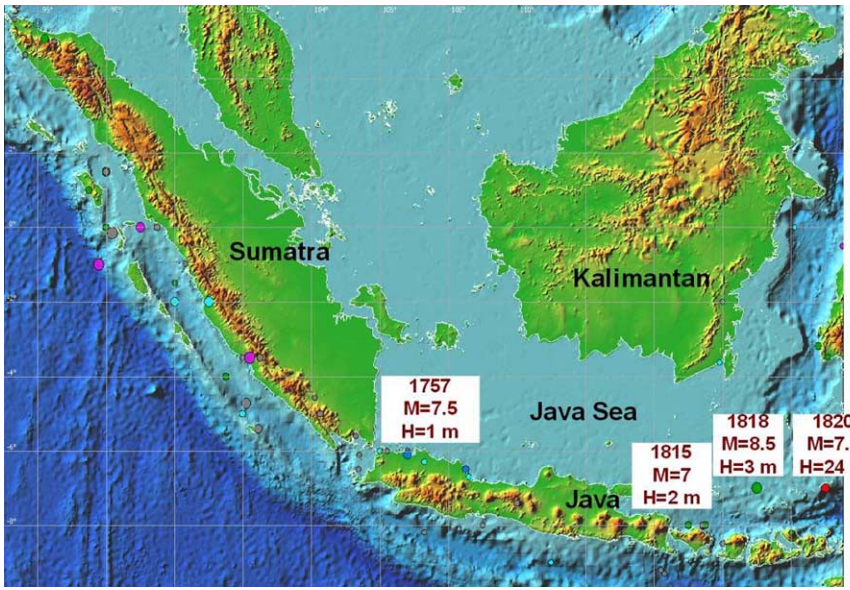

Fig. 1. Map of the Java Sea with the location of strong tsunamis generated by earthquakes (M is the Richter magnitude, and H is maximum runup height in m).

displacement (in m) with an interval of 1 h demonstrating the tsunami propagation in the Java Sea are given in Fig. 2 (initial height 5 m, the friction is included). It is clearly seen the elliptic divergence of the wave front with decreasing of its height, and formation of the negative displacement in the source according to the classic solution of the 2D linear wave equation. The wave approaches to the coast of Java for 90 min, and to the opposite coast (Kalimantan) for 180 min.

The computed distribution of the maximum cret amplitude characterizes the directivity of the tsunami propagation (Fig. 3). Tsunami waves propagate mainly in the direction of the small axis of the elliptic source, as it follows from the well-known solutions of the linear wave equation, they applied in the tsunami theory [9,12].

To investigate the role of nonlinear effects, several runs have been performed. The first run is the weak-amplitude wave (initial displacement, 1 m) and the friction term is ignored. The second run is the large-amplitude wave (initial displacement 5 m) and the friction term is again ignored. The third run is the large-amplitude wave taking into account the nonlinear friction. Results of computing of the elevation time series for these three variants on various distances from the source to south and north along the longitude are displayed in Figs. 4 and 5.

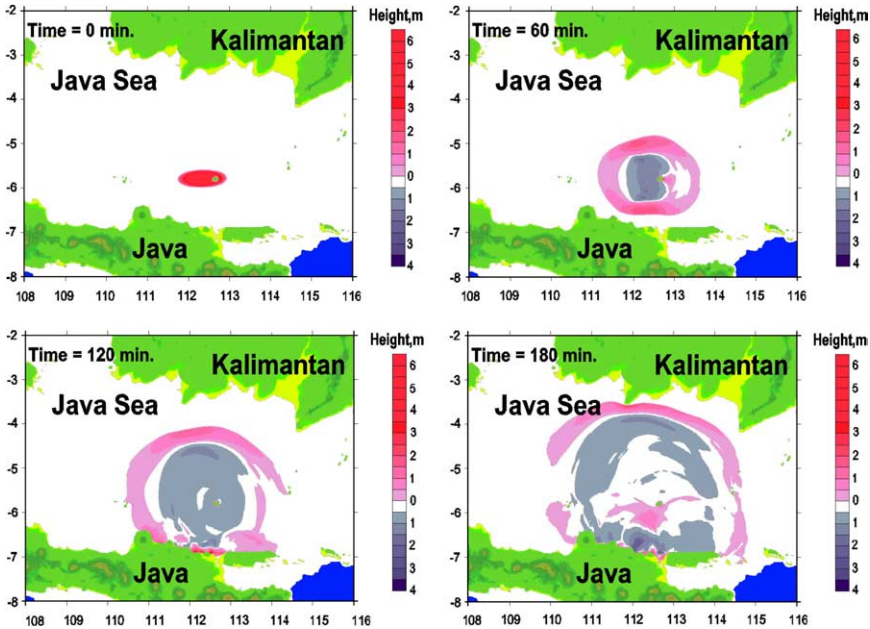

Fig. 2. Snapshots of tsunami propagation in the Java Sea with an interval of 1 h (numbers on axes are geographic degrees in latitude and longitude).

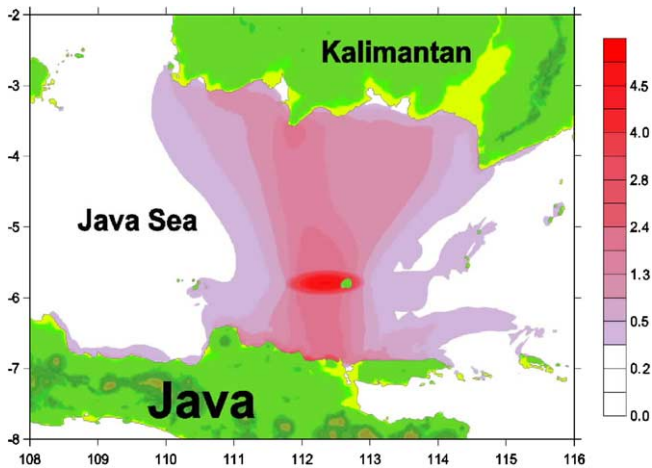

Fig. 3. Computed distribution of the maximum positive wave amplitude (in meters) in the Java Sea. The red ellipse shows the location of the tsunami source.

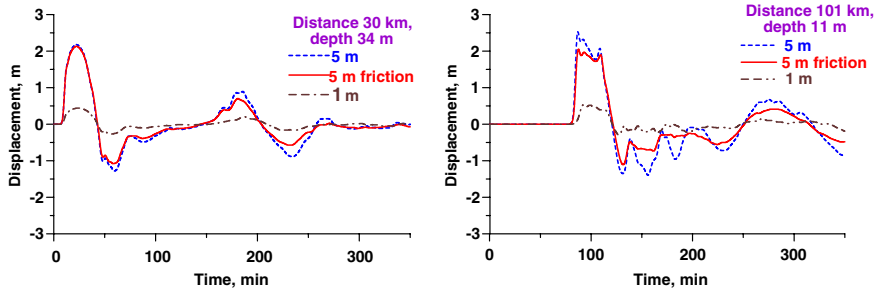

Fig. 4. Time series of the computed waves propagated to the south from the source.

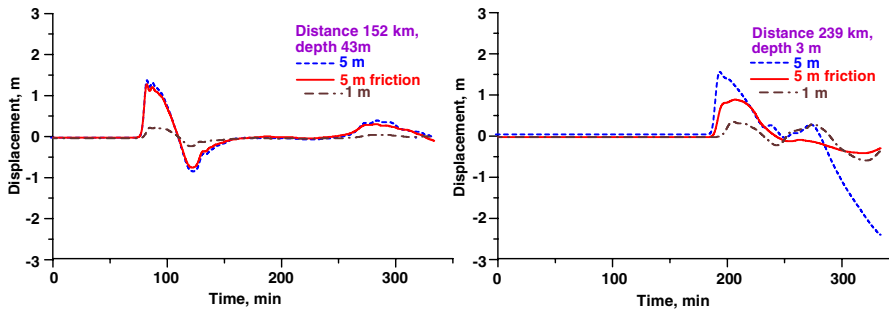

Fig. 5. Time series of the computed waves propagated to the north from the source.

First of all, all pictures demonstrate the reflection of the wave from the nearest coast where the full reflection condition is applied. On large distances from the source, the incident and reflected waves are not separated forming the complex time record. On small distances from the source (approximately equaled to the wavelength as it is shown in Fig. 4, left), the wave shape is almost symmetrical and repeats the initial water displacement with approximately a half of amplitude as in the 1D problem. The effect of the bottom friction on such short distances is not important. On the large distances, wave shape becomes more nonlinear with the steepest front. The difference in the steepness of the wave front is very visible on small depth; see Fig. 5 (right). The triangle shock-like shape forms on relative large depth of 40 m (Fig. 5, left). The bottom friction influences mainly on the negative waves (troughs) due to decreasing of the total depth under the trough; see, for instance Fig. 5 (right).

Given example demonstrates that the nonlinear effects are manifested in shallow water on the distance 150 km and more, and such situation can be realized in the large shallow seas. We would like to mention again that to compare with well-known effect of the tsunami wave breaking on the shore or when

tsunami entries in the river (see, for instance, [17]), this mechanism of the bore forming "works" on finite depth (but on large distances), and the tsunami wave can have the bore-like shape in the sea on finite depth.

3. Nonlinear effects at the wave separation in the source

On small distances from the source, the nonlinear friction is negligible. Also, let us assume that the basin depth varies weakly in the source (it is not common rule for tsunami). For simplicity, the divergence of the wave field can be ignored. In this case, the initial system (2) reduces to

$$\frac{\partial u}{\partial t} + u\frac{\partial u}{\partial t} + g\frac{\partial \eta}{\partial x} = 0, \tag{3a}$$

$$\frac{\partial \eta}{\partial t} + \frac{\partial}{\partial x}[(h+\eta)u] = 0, \tag{3b}$$

with initial conditions

$$\eta(x,0) = \eta_{\text{in}}(x), \quad u(x,0) = 0. \tag{4}$$

The solution of the linearised system (3) is well-known, and it describes two waves propagated in the opposite directions

$$\eta(x,t) = \frac{1}{2}[\eta_{\text{in}}(x - c_0 t) + \eta_{\text{in}}(x + c_0 t)], \quad c_0 = \sqrt{gh}. \tag{5}$$

To solve the nonlinear system (3), we will use the Riemann's invariants

$$I_{\pm} = u \pm 2\lfloor\sqrt{g(h+\eta)} - \sqrt{gh}\rfloor, \tag{6}$$

which are, evidently, retained at the characteristics

$$c_{\pm} = \pm\sqrt{gh} + \frac{3}{4}I_{\pm} + \frac{1}{4}I_{\mp}. \tag{7}$$

At the initial time moment, since $u(x,0) = 0$, and any of the invariants, e.g., I_+, equals

$$I_+(t=0) = 2\lfloor\sqrt{g[h+\eta_{\text{in}}(x)]} - \sqrt{gh}\rfloor. \tag{8}$$

After a wave propagating to the right leaves the source, the invariants gain the following values:

$$I_+(t) = 2\lfloor\sqrt{g[h+\eta(x',t)]} - \sqrt{gh}\rfloor, \quad I_- = 0, \tag{9}$$

where the wave coordinate should be determined from the system of the characteristic equations

$$\frac{\mathrm{d}x}{\mathrm{d}t} = c_+, \quad \frac{\mathrm{d}x}{\mathrm{d}t} = c_-. \tag{10}$$

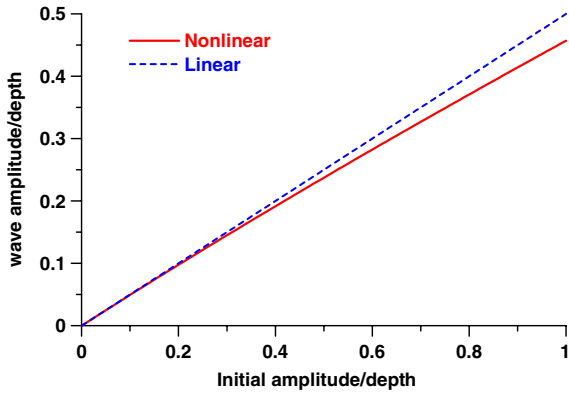

Fig. 6. Amplitude of the wave outside of the source area.

The solution of the characteristic equation analytically is the difficult task, and we could not find explicity the shape of the wave leaved the source. But its amplitude can be found from the conservation of maximum value I_+; it leads

$$A = \frac{A_{\text{in}}}{4} + \frac{1}{2}\left[\sqrt{1 + \frac{A_{\text{in}}}{h}} - 1\right], \tag{11}$$

where A and A_{in} are the wave amplitude and initial amplitude consequently. Fig. 6 plots this function in dimensionless variables (A/h). In the case of weak amplitudes, it yields the known equation: $A = A_{\text{in}}/2$. However, even for high amplitudes ($A_0 = h$) the difference from Eq. (10) is relatively small ($A = 0.457h$ instead of $0.5h$). Therefore, in the framework of the shallow-water theory nonlinear effects at the breakdown stage of the initial disturbance can be neglected. As it can be expected, the divergence of the wave front in the 2D case will also reduce the nonlinear effects. In the simplified form of the cycle source with radius, R, the amplitude of linear wave outside of the source is described by

$$A(r) = \frac{A_{\text{in}}}{2}\left(\frac{r}{R}\right)^{-1/2}. \tag{12}$$

4. Approximated solutions for the nonlinear wave propagation

On the large distances from the source the variable depth as well as nonlinear friction will influence on the wave evolution. The system (2) in this case reduces to

$$\frac{\partial u}{\partial t}+u\frac{\partial u}{\partial x}+g\frac{\partial \eta}{\partial x}=-\frac{k}{2h(x)}u|u|, \tag{13a}$$

$$\frac{\partial \eta}{\partial t}+\frac{\partial}{\partial x}[(h(x)+\eta)u]=0. \tag{13b}$$

It is convenient to use again the Riemann invariants (5) instead of u and η, and system (13) can be re-written

$$\frac{\partial I_{\pm}}{\partial t}+c_{\pm}(h,I_{+},I_{-})\frac{\partial I_{\pm}}{\partial x}=\mp\left(\frac{3}{4}I_{\pm}+\frac{1}{4}I_{\mp}\right)\sqrt{\frac{g}{h}}\frac{\mathrm{d}h}{\mathrm{d}x}-\frac{k}{2h}\frac{I_{+}+I_{-}}{2}\left|\frac{I_{+}+I_{-}}{2}\right|. \tag{14}$$

In the case of the smooth bottom profile and weak dissipation, the reflected wave characterized by I_{-} will be also weak, and it can be neglected. In the one-wave approximation (see for instance, [5] for rigorous description of such asymptotic procedures, and also [4]) the basic equation of the first order is

$$\frac{\partial I_{+}}{\partial t}+c_{\pm}(h,I_{+},0)\frac{\partial I_{+}}{\partial x}=-\sqrt{\frac{g}{h}}\frac{\mathrm{d}h}{\mathrm{d}x}\frac{3}{4}I_{+}-\frac{k}{8h}I_{+}|I_{+}|. \tag{15}$$

Taking into account the relation with initial physical variables, this equation can be written in the final form

$$\frac{\partial u}{\partial t}+\left[\sqrt{gh(x)}+\frac{3}{2}u\right]\frac{\partial u}{\partial x}=-\sqrt{\frac{g}{h}}\frac{\mathrm{d}h}{\mathrm{d}x}\frac{3u}{4}-\frac{k}{4h}u|u|, \tag{16a}$$

$$u=2\lfloor\sqrt{g(h+\eta)}-\sqrt{gh}\rfloor. \tag{16b}$$

The partial differential equation of the first order is equivalent to the pair of the ordinary differential equations

$$\frac{\mathrm{d}u}{\mathrm{d}x}=-\frac{3u}{4}\frac{\sqrt{\frac{g}{h}}\frac{\mathrm{d}h}{\mathrm{d}x}}{\sqrt{gh}+\frac{3u}{2}}-\frac{ku|u|}{4h\left(\sqrt{gh}+\frac{3u}{2}\right)}, \tag{17a}$$

$$\frac{\mathrm{d}t}{\mathrm{d}x}=\frac{1}{\sqrt{gh}+\frac{3u}{2}}. \tag{17b}$$

The first Eq. (17a) describes the amplitude evolution, and the second one (17b)—travel time. The various solutions of the amplitude equation can be found for the given bottom profile.

4.1. Even bottom, no friction

In this case the solution of (16) or (17) is exact and describe the simple wave

$$\eta(x,t)=\eta_{0}\left[t-\frac{x}{3\sqrt{g(h+\eta)}-2\sqrt{gh}}\right], \tag{18}$$

where $\eta_0(t)$ is the wave left the source area, its amplitude is found in Section 3. The wave amplitude does not change with distance, but its steepness is increased with distance, and this expression can be found from (18)

$$\frac{\partial\eta}{\partial t} = \frac{\mathrm{d}\eta_0/\mathrm{d}\xi}{1 + x\frac{\mathrm{d}(1/V)}{\mathrm{d}\xi}}, \quad V(\eta) = 3\sqrt{g(h+\eta)} - 2\sqrt{\mathrm{d}h}, \tag{19}$$

where ξ is an argument of η_0. On the wave front, $\mathrm{d}(1/V)/\mathrm{d}\xi$ is negative, and the wave steepness is increased up to infinity, when the wave breaks. This distance is simple determined if the initial wave shape is known

$$L_{\mathrm{br}} = \frac{1}{\max\left(-\frac{\mathrm{d}(1/V)}{\mathrm{d}t}\right)}. \tag{20}$$

In particular, the weak-amplitude sine wave breaks at distance

$$L_{\mathrm{br}} = \frac{2h\sqrt{gh}}{3A_0\omega}. \tag{21}$$

4.2. Even bottom, nonlinear friction

In this case the amplitude equation (17a) is integrated

$$-\frac{kx}{4h} = \sqrt{gh}\left(\frac{1}{U_0} - \frac{1}{U(x)}\right) + \frac{3}{2}\log\frac{U(x)}{U_0}, \tag{22}$$

where U_0 is the amplitude of u. In the weak-amplitude limit, this solution can be done directly for the wave amplitude

$$A(x) = \frac{A_0}{1 + \frac{kA_0x}{8h^2}}, \tag{23}$$

and the wave amplitude does not depend on the initial amplitude for large distance from the source. The wave damps very strongly in the shallowest area as it was demonstrated numerically in Section 2. The second equation (17b) is also integrated, and in the weak-amplitude limit the travel time is

$$\sqrt{gh}(t - t_0) = x - \frac{12h}{k}\log\left(1 + \frac{kA_0x}{8h^2}\right). \tag{24}$$

In fact, A_0 and t_0 characterize the current value of $\eta_0(t)$, and therefore, the various parts of the wave profile propagate with different speeds. The curves (t, x) will cross on large distances meaning that the wave breaks for any values of the initial amplitude. It is the main difference with the linear friction when weak-nonlinear waves will not break due to strong exponential damping [20].

4.3. Variable bottom, no friction

In this case, the amplitude equation is integrated in explicit form:

$$h^5 F(v) = \text{const}, \quad F(v) = v^4(5+3v)^5, \\ v = u/\sqrt{gh} = 2(\sqrt{1+A/h}-1). \tag{25}$$

In the weak-amplitude limit from (25) follows the Green formula

$$U \sim h^{-3/4}, \quad A \sim h^{-1/4}. \tag{26}$$

According to (25) nonlinearity leads to the slowest variation of the wave amplitude to compare with the linear waves.

4.4. Cylindrical divergence

The directivity diagram of wave propagation (Fig. 3) shows that the 2D effects are important for the tsunami waves far from the source. The analytical solution of the 2D shallow-water equations is a difficult task, and here we consider the one example of the cylindrical nonlinear waves far from the source. In this case the approximated equation can be derived similarly (16), see Engelbrecht et al. [5] for mathematical details, and in the case of weak-amplitude waves it is (no friction, no bottom variability)

$$\frac{\partial \eta}{\partial t} + c_0\left(1+\frac{3\eta}{2h}\right)\frac{\partial \eta}{\partial r} + \frac{c_0\eta}{2r} = 0. \tag{27}$$

In fact, there are two small parameters: nonlinearity, η/h and divergence, R/r, where R is the source radius. Introducing the linear travel time $\tau = t - x/c_0$, in the first order on these parameters, Eq. (27) can be re-written as

$$\frac{\partial \eta}{\partial r} - \frac{3\eta}{2hc_0}\frac{\partial \eta}{\partial \tau} + \frac{\eta}{2r} = 0. \tag{28}$$

It can be solved exactly

$$\eta(\tau, r) = \sqrt{\frac{R}{r}}\eta_0\left(\tau + \frac{3\eta r}{hc_0}\right), \tag{29}$$

where $\eta_0(t)$ is the wave left the source. The wave amplitude decreases with distance as $r^{-1/2}$, as in the linear cylindrical wave. More important is that the front steepness is increased with distance

$$\frac{\partial \eta}{\partial t} = \sqrt{\frac{R}{r}}\frac{\frac{\mathrm{d}\eta_0}{\mathrm{d}\xi}}{\left[1 - \frac{3\sqrt{Rr}}{hc_0}\frac{\mathrm{d}\eta_0}{\mathrm{d}\xi}\right]}, \tag{30}$$

where ξ is an argument of η_0 (it is the time when the wave left the source). For large distance, the denominator tends to zero, and the wave steepness increased

infinity—the wave breaks. The distance of the wave breaking is found from (30)

$$r_{br} = \frac{h^2 c_0^2}{9R \max[(\mathrm{d}\eta_0/\mathrm{d}\xi)]^2}. \tag{31}$$

5. Comparison with numerical simulations of tsunami waves

Let us analyze the results of the numerical simulations of the tsunami waves in the Java Sea and the possibility to explain them with the approximated ana-

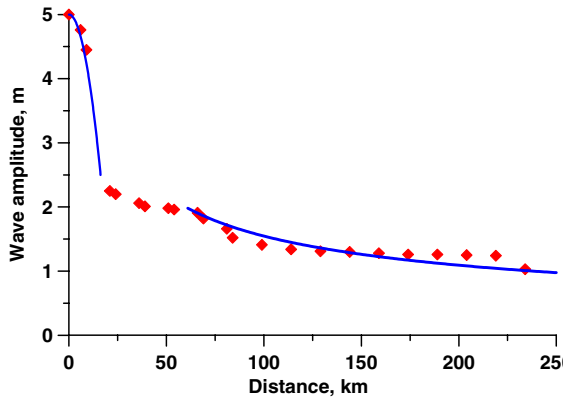

Fig. 7. Wave amplitude versus the longitude distance (theory—solid line and numerical simulations—rhombs).

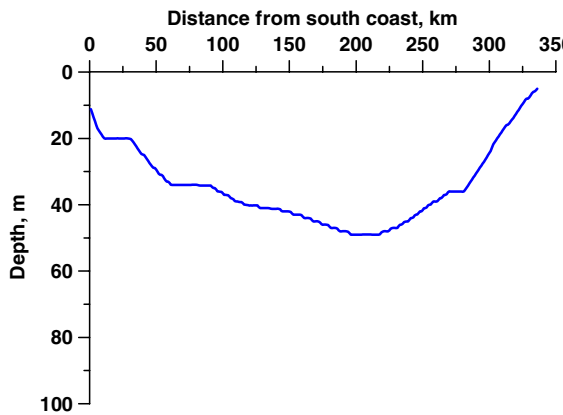

Fig. 8. Bottom profile along the longitude (the epicenter is located on distance 101 km from south).

lytical solutions. Fig. 7 displays the maximum crest amplitude of the tsunami wave along the longitude. On the small distances from the source, maximum wave amplitude repeats the initial wave profile according to the linear solution of the 1D problem (5) or nonlinear correction (11), which is weak. The results of the numerical simulation correspond to the theoretical prediction very well. On the large distances, the divergence effects become important and the wave transforms to the cylindrical one, and its amplitude is proportional to $r^{-1/2}$; see (12). The variable bathymetry leads to the deviation of numerical points from the theoretical curve, but this effect is weak, because the water depth is varied weakly, from 30 to 40 m, except the coastal locations (Fig. 8).

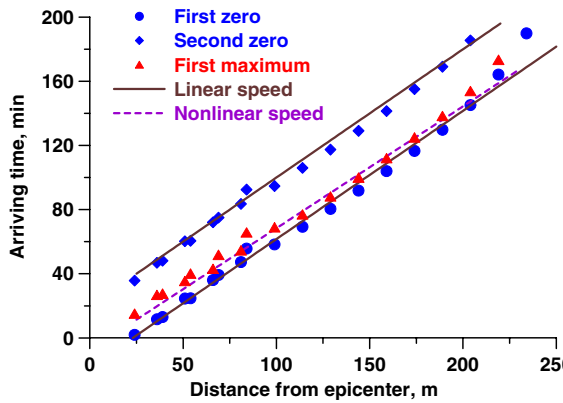

Fig. 9. Arriving time of the wave front (first zero), first maximum and second zero: points—computing, solid lines—theoretical line (17b).

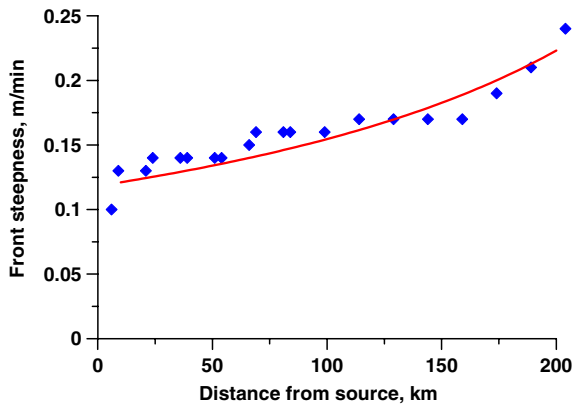

Fig. 10. The front steepness versus the distance from the source: rhombs—numerical results, solid line—theoretical line (19).

The approaching times of the wave front (the "first zero" of the computed), point of the maximum amplitude and the second zero (the end of the first crest) are shown in Fig. 9. The zero points move with the linear speed calculated for mean depth 44 m, and the first maximum—with nonlinear speed, exceeded the linear speed on 5%. The bottom variations induce again the scattering of the computed points, but they are grouped around the theoretical lines. It is clearly seen the increasing of the nonlinear steepness of the wave front with distance in spite of the cylindrical divergence of the wave front; see also Fig. 10. The theoretical line is found using the 1D theory based on (19).

6. Conclusion

The nonlinear hyperbolic shallow-water system is an effective tool to compute the propagation and runup of the tsunami waves. Very often the numerical simulations of the tsunami propagation from the source are performed for relative large depths (more 10–20 m) and nonlinear effects are not manifested for such depths. The reproducing of the nonlinear effects in the tsunami wave field requires high-resolution of the bathymetric maps and long computations, and it is why the nonlinear theory of water waves applied mainly to describe the runup stage, but not the tsunami propagation. The given paper demonstrates the appearance of the nonlinear effects for propagation stage in the shallowest seas like the Java Sea. Taking into account the 2D character of the wave field and the 2D variability of the seabed relief the possibilities of analytical methods are limited in the general case. We chosen the relative even part of the Java Sea and shown that the wave characteristics can be calculated analytically. In fact, we used the matching of 1D and 2D formulas for the wave amplitude in the basin of constant depth, and the 1D approach to describe the steepness of the wave front. The analytical results are in good agreement with the computed data. Authors believe that this approach will be effective for many shallowest basins of the World Ocean.

We plan to investigate the role of solitons in the dynamics of the tsunami waves; this problem was discussed early theoretically only [7,8].

Acknowledgements

The research was supported by the INTAS grant (01-2156) and EGIDE French–Russian program (04500YH). The partial support from the RFBR grant (05-05-64265) and INTAS (03-51-4286) for EP and RFBR grant (03-05-64975) for AK is used.

References

[1] T. Bryant, Tsunamis, Cambridge University Press, 2001.
[2] G.F. Carrier, T.T. Wu, H. Yeh, Tsunami run-up and draw-down on a plane beach, J. Fluid Mech. 475 (2003) 79–99.
[3] B.H. Choi, E. Pelinovsky, K.O. Kim, J.S. Lee, Simulation of the trans-oceanic tsunami propagation due to the 1883 krakatau volcanic Eruption, Natural Hazards Earth Syst. Sci. 3 (5) (2003) 321–332.
[4] J.-G. Caputo, Y.A. Stepanyants, Bore formation, evolution and disintegration into solitons in shallow inhomogeneous channels, Nonlinear Process. Geophys. 10 (2003) 407–424.
[5] J.K. Engelbrecht, V.E. Fridman, E.N. Pelinovsky, Nonlinear Evolution Equation, Pitman Research Notes in Mathematics Series, No. 180, London, Longman, 1988.
[6] C. Goto, Y. Ogawa, N. Shuto, N. Imamura, Numerical method of tsunami simulation with the leap-frog scheme (IUGG/IOC Time Project), IOC Manual, UNESCO, 1997, No. 35.
[7] J.L. Hammack, A note on tsunamis: Their generation and propagation in an ocean of uniform depth, J. Fluid Mech. 60 (1973) 769–799.
[8] N.R. Mirchina, E.N. Pelinovsky, Solitons in the tsunami problem, in: R. Sagdeev (Ed.), Nonlinear and Turbulent Processes in Physics, vol. 2, Academic Publisher, 1984, pp. 973–978.
[9] T. Murty, Seismic Sea Waves—Tsunamis, Bull. Dep. Fisheries, Canada, 1977.
[10] J. Park, K. Anderson, R. Aster, R. Butler, T. Lay, D. Simpson, Global seismographic network records the great Sumatra—Andaman earthquake, EOS 86 (6) (2005) 57–64.
[11] E. Pelinovsky, Nonlinear hyperbolic equations and runup of huge sea waves, Appl. Anal. 57 (1995) 63–84.
[12] E.N. Pelinovsky, Hydrodynamics of Tsunami Waves, Institute of Applied Physics Press, Nizhny Novgorod, 1996.
[13] E. Pelinovsky, R. Mazova, Exact analytical solutions of nonlinear problems of tsunami wave run-up on slopes with different profiles, Natural Hazards 6 (1992) 227–249.
[14] E. Pelinovsky, C. Kharif, I. Riabov, M. Francius, Modelling of tsunami propagation in the vicinity of the French coast of the mediterranean, Natural Hazards 25 (2) (2002) 135–159.
[15] K. Satake, Linear and nonlinear computations of the 1992 Nicaragua earthquake tsunamis, Pure Appl. Geophys. 144 (1995) 455–470.
[16] C.E. Synolakis, The runup of solitary waves, J. Fluid Mech. 185 (1987) 523–545.
[17] Y. Tsuji, T. Yanuma, I. Murata, C. Fujiwara, Tsunami ascending in rivers as an undular bore, Natural Hazards 4 (1991) 257–266.
[18] N. Zahibo, E. Pelinovsky, A. Yalciner, A. Kurkin, A. Koselkov, A. Zaitsev, The 1867 Virgin island tsunami: Observations and modelling, Oceanol. Acta 26 (5–6) (2003) 609–621.
[19] A. Yalciner, E. Pelinovsky, T. Talipova, A. Kurkin, A. Kozelkov, A. Zaitsev, Tsunamis in the Black Sea: Comparison of the historical, instrumental and numerical data, J. Geophys. Res. 109 (C12, C12023) (2004), doi:10.1029/2003JC002113.
[20] Y.H. Wu, J.-W. Tian, Mathematical analysis of long-wave breaking on open channels with bottom friction, Ocean Eng. 26 (2000) 187–201.
[21] A. Zaitsev, A. Kurkin, B. Levin, E. Pelinovsky, A.C. Yalciner, Yu. Troitskaya, S. Ermakov, Modeling of propagation of the catastrophic tsunami (December 26, 2004) in the Indian Ocean, Doklady Earth Sci. 403 (3) (2005).